Smart Structures and Systems, *Vol. 13, No. 4 (2014) 637-657*
DOI: http://dx.doi.org/10.12989/sss.2014.13.4.637

A dynamic analysis of three-dimensional functionally graded beams by hierarchical models

Gaetano Giunta[*1], Yao Koutsawa[1a], Salim Belouettar[1b] and Adriano Calvi[2c]

[1]*Centre de Recherche Public Henri Tudor, 29, av. John F. Kennedy, L-1855, Luxembourg-Kirchberg, Luxembourg*
[2]*ESTEC - European Space Agency, P.O. Box 299, 2200 AG, Noordwijk, The Netherlands*

(Received April 13, 2013, Revised November 25, 2012, Accepted November 30, 2012)

Abstract. This paper presents a dynamic analysis of three-dimensional beams. Structures made of functionally graded materials are considered. Several higher-order as well as classical theories are derived by means of a compact notation for the a-priori expansion order of the displacement field over the beam cross-section. The governing differential equations and boundary conditions are obtained in a condensed nuclear form that does not depend on the kinematic hypotheses. The problem is, then, exactly solved in space by means of a Navier-type solution, whereas time integration is performed by means of Newmark's solution scheme. Slender and short simply supported beams are investigated. Results are validated towards three-dimensional FEM results obtained via the commercial software ANSYS. Numerical investigations show that good accuracy can be obtained through the proposed formulation provided that the appropriate expansion order is considered.

Keywords: three-dimensional beam structures; functionally graded materials; dynamic analysis

1. Introduction

Functionally Graded Materials (FGMs) represent very attractive solutions due to the continuous and gradual change of their properties along desired spatial directions. A multi-functional structural response can be obtained by means of a proper combination of the different material components resulting in a broadened structural design space. As far as structures are concerned, beams play an important role in research since they can be used to idealise many primary and secondary structural elements, such as aircraft wings, helicopter rotor blades or robot arms. In particular, their dynamic behaviour is of major concern in several applications. The dynamic response of three-dimensional FGM beam structures is, therefore, an important and up-to-date research topic.

A brief overview of some recent works about FGMs and their dynamic analysis follows. An interesting historical overview on FGMs can be found in Koizumi (1997). A general account of

∗Corresponding author, Ph. D., E-mail: gaetano.giunta@tudor.lu
[a] Ph.D., E-mail: yao.koutsawa@tudor.lu
[b] Ph.D., E-mail: salim.belouettar@tudor.lu
[c] Ph.D., E-mail: adriano.calvi@esa.int

http://www.techno-press.org/?journal=sss&subpage=8 ISSN: 1738-1584 (Print), 1738-1991 (Online)

FGMs (design, fabrication and applications) was presented by Suresh and Mortensen (1998), Miyamoto *et al*. (1999), Watanabe *et al*. (2003) and Birman and Byrd (2007). A review of classical micro-mechanical approaches such as self-consistent schemes, see Hill (1965), differential schemes, Mori-Tanaka's (1973) method and concentric cylinder models can be found in Aboudi (1991), Nemat-Nasser and Hori (1993) and Zuiker and Dvorak (1994). To the best of authors' knowledge, one of the first micro-mechanical approaches for FGMs was proposed by Wakashima and Tsukamoto (1990). Pindera *et al*. (1995) demonstrated that classical methods cannot be profitably applied to FGMs since they decouple the local response from the global one. A higher-order theory for FGMs based on a volumetric averaging approach that explicitly couples micro- and macro-scale with spatially varying micro-structures in one, two and three orthogonal directions was presented by Aboudi *et al*. (1994, 1996, 1999).

As far as structural mechanics is concerned, Bui *et al*. (2013) investigated the free and forced vibration of sandwich beams embedding a FGM core using a radial point interpolation meshless method. The Cartesian transformation method was used for computing the integrals over the beam spatial domain. Newmark's (1959) time discretisation scheme was employed. A non-linear forced vibration analysis of FGM clamped beams was carried out by Shooshtari and Rafiee (2011). Geometric non-linearities were considered in a von Kármán sense and the external load was harmonic. An analytical solution was presented. Temperature dependent material properties were considered by Azadi (2011) for the free and forced vibration of FGM beams. Na *et al*. (2009) investigated the dynamic response of functionally graded blades. Rotating thin-walled beams with a box cross-section subjected to thermo-mechanical loads were considered. Analyses were carried out considering several geometric (taper ratio, twisting and setting angle), material (volume fraction) and load (temperature gradient) parameters. Şimşek *et al*. (2009, 2012) studied the dynamic behaviour of through-the-thickness and axially graded beams by means of Euler-Bernoulli classical model accounting for moving harmonic loads. The load amplitude was considered to vary harmonically. Elastically connected double-functionally graded beam systems were investigated in Şimşek and Cansiz (2012). Şimşek (2010) applied Euler-Bernoulli's, Timoshenko's and third-order shear deformation theories to the study of the forced vibrations of FGM beams due to a moving mass. Khalili *et al*. (2010) considered the dynamic response of FGM Euler-Bernoulli beams under moving loads where spatial and time derivatives were approximated by means of Rayleigh-Ritz and differential quadrature methods, respectively. The load was represented by a mass moving along the beam axis to introduce a further inertial contribution. Results were compared with solution obtained using Newmark's and Wilson's algorithms. Yang et al. (2008) considered the free and forced vibrations of FGM cracked beams by means of analytical solutions. Euler-Bernoulli's kinematic model was used. The beams were loaded by an axial compressive force and a transversal one that was moving along the axial direction. Several boundary conditions were accounted for. The forced response was obtained via the modal expansion method.

The forced vibrations of three-dimensional FGM beams are investigated within this paper by a unified formulation. This formulation has been previously derived for plates and shells, see Carrera (2003) and Carrera and Giunta (2009a, b, 2011), and extended to three-dimensional beam structures in Carrera and Giunta (2010), Carrera *et al*. (2010, 2011) and Giunta *et al*. (2010, 2011a, 2013a, b). To the best of authors' knowledge, the proposed formulation was first applied to the dynamic analysis of homogeneous and isotropic beams in Carrera *et al*. (2013). The present article stems from the free-vibration analysis of FGM beams presented in Giunta *et al*. (2011b). The variation of the material stiffness coefficients and density with respect to the cross-section

coordinates is expressed as a bi-dimensional Lagrange approximation using Newton's series expansion and Chebyshev points, see Philips (2003). In such a manner, the derivation does not depend on the particular material gradation law. The Principle of Virtual Displacement is used for deriving the governing differential equations and the corresponding boundary conditions. They are obtained as a "fundamental nucleo" that does not depend on the displacement field approximation order. Higher-order beam theories accounting for non-classical effects, such as transverse shear and cross-section in- and out-of-plane warping, are formulated straightforwardly. The governing equations in the spatial domain are solved exactly using a Navier-type strong form solution. Simply supported beams are, therefore, investigated. As far as the time domain problem is concerned, several procedures have been developed to carry the integration out. A thorough discussion on analytical procedures, semi-discretisation processes and single- as well as multi-step algorithms is presented in Bathe (2006), Zienkiewicz *et al*. (2005) and Hughes (2000). Time discretisation is here done by means of the well-known Newmark scheme (1959). Slender and deep beams are investigated. Cross-sections are made of a bi-dimensional FGM. A power law function is assumed for the material gradation. The proposed models are validated towards three-dimensional FEM solutions. Numerical results show that very accurate results can be obtained with a reduced computational effort when compared with traditional three-dimensional FEM solutions.

2. Preliminaries

A beam is a structure whose axial extension (l) is predominant when compared with any other dimension orthogonal to it. The cross-section (Ω) is identified by intersecting the beam with planes that are orthogonal to its axis. A Cartesian reference system is adopted: y- and z-axis are two orthogonal directions lying on Ω. The x coordinate is coincident with the axis of the beam. It is bounded such that $0 \le x \le l$.

Beam geometry and reference system are presented in Fig. 1. The cross-section is considered to be constant along x. The displacement field is

$$\mathbf{u}^T\left(x,y,z\right)=\left\{u_x\left(x,y,z\right)\quad u_y\left(x,y,z\right)\quad u_z\left(x,y,z\right)\right\} \tag{1}$$

in which u_x, u_y and u_z are the displacement components along the x-, y- and z-axis, respectively. Superscript 'T' represents the transposition operator. Stress, $\boldsymbol{\sigma}$, and strain, $\boldsymbol{\varepsilon}$, vectors are grouped into vectors σ_n, ε_n that lie on the cross-section

$$\boldsymbol{\sigma}_n^T=\left\{\sigma_{xx}\quad\sigma_{xy}\quad\sigma_{xz}\right\}\quad\boldsymbol{\varepsilon}_n^T=\left\{\varepsilon_{xx}\quad\varepsilon_{xy}\quad\varepsilon_{xz}\right\} \tag{2}$$

and $\boldsymbol{\sigma}_p$, $\boldsymbol{\varepsilon}_p$ lying on planes orthogonal to Ω

$$\boldsymbol{\sigma}_p^T=\left\{\sigma_{yy}\quad\sigma_{zz}\quad\sigma_{yz}\right\}\quad\boldsymbol{\varepsilon}_p^T=\left\{\varepsilon_{yy}\quad\varepsilon_{zz}\quad\varepsilon_{yz}\right\} \tag{3}$$

Under the hypothesis of linear analysis, the following strain-displacement geometrical relations hold

$$\begin{aligned} \varepsilon_n^T &= \left\{ u_{x,x} \quad u_{x,y}+u_{y,x} \quad u_{x,z}+u_{z,x} \right\} \\ \varepsilon_p^T &= \left\{ u_{y,y} \quad u_{z,z} \quad u_{y,z}+u_{z,y} \right\} \end{aligned} \tag{4}$$

Subscripts ‘ x ’, ‘ y ’ and ‘ z ’, when preceded by comma, represent derivation with respect to the corresponding spatial coordinate. A compact vectorial notation can be adopted for Eq. (4)

$$\begin{aligned} \boldsymbol{\varepsilon}_n &= \mathbf{D}_{np}\mathbf{u} + \mathbf{D}_{nx}\mathbf{u} \\ \boldsymbol{\varepsilon}_p &= \mathbf{D}_p\mathbf{u} \end{aligned} \tag{5}$$

where $\mathbf{D}_{np}$, $\mathbf{D}_{nx}$, and $\mathbf{D}_p$ are the following differential matrix operators

$$\mathbf{D}_{np} = \begin{bmatrix} 0 & 0 & 0 \\ \dfrac{\partial}{\partial y} & 0 & 0 \\ \dfrac{\partial}{\partial z} & 0 & 0 \end{bmatrix} \quad \mathbf{D}_{nx} = \mathbf{I}\frac{\partial}{\partial x} \quad \mathbf{D}_p = \begin{bmatrix} 0 & \dfrac{\partial}{\partial y} & 0 \\ 0 & 0 & \dfrac{\partial}{\partial z} \\ 0 & \dfrac{\partial}{\partial z} & \dfrac{\partial}{\partial y} \end{bmatrix} \tag{6}$$

and $\mathbf{I}$ is the unit matrix. Under the hypothesis of linear elastic materials, the generalised Hooke law holds. According to Eqs. (2) and (3), it reads

$$\begin{aligned} \boldsymbol{\sigma}_p &= \mathbf{C}_{pp}\boldsymbol{\varepsilon}_p + \mathbf{C}_{pn}\boldsymbol{\varepsilon}_n \\ \boldsymbol{\sigma}_n &= \mathbf{C}_{np}\boldsymbol{\varepsilon}_p + \mathbf{C}_{nn}\boldsymbol{\varepsilon}_n \end{aligned} \tag{7}$$

In the case of isotropic FGMs, matrices $\mathbf{C}_{pp}$, $\mathbf{C}_{pn}$, $\mathbf{C}_{np}$ and $\mathbf{C}_{nn}$ in Eq. (7) are

$$\mathbf{C}_{pp} = \begin{bmatrix} C_{22} & C_{23} & 0 \\ C_{23} & C_{33} & 0 \\ 0 & 0 & C_{44} \end{bmatrix} \quad \mathbf{C}_{pn} = \mathbf{C}_{np}^T = \begin{bmatrix} C_{12} & 0 & 0 \\ C_{13} & 0 & 0 \\ 0 & 0 & 0 \end{bmatrix} \quad \mathbf{C}_{nn} = \begin{bmatrix} C_{11} & 0 & 0 \\ 0 & C_{66} & 0 \\ 0 & 0 & C_{55} \end{bmatrix} \tag{8}$$

In order to make the software implementation of the proposed models independent from the particular gradation law, a Lagrange approximation over N_p Chebyshev points along y and z co-ordinates based on Newton’s series expansion is assumed for the material stiffness coefficients in Eq. (8)

$$C_{ij}(x,y) \approx \omega_\xi(y)\omega_\eta(z) C_{ij}\left[y_0, y_1, \ldots, y_\xi; z_0, z_1, \ldots, z_\eta\right] \quad \text{with } \xi,\eta = 0,1,\ldots,N_p \tag{9}$$

being

$$\omega_m(\zeta) = \begin{cases} 1 & m = 0 \\ \displaystyle\prod_{n=0}^{m-1} (\zeta - \zeta_n) & m \in \left[1, N_p\right] \end{cases} \tag{10}$$

Chebyshev's points are defined over the domain $[-1,+1]$ via the following equation

$$\zeta_m = \cos\left(\frac{m\pi}{N_p}\right) \quad \text{with} \quad m = 0,1,\ldots,N_p \tag{11}$$

These points are then mapped into the cross-section domain via a variables transformation. Terms $C_{ij}[\ldots;\ldots]$ are the divided differences computed from the functions $C_{ij} = C_{ij}(y,z)$, see Philips (2003). These latter depend on the particular gradation law chosen for the numerical investigations and they can be obtained via numerical or analytical homogenisation analyses. In this article, a power gradation law of the volume fraction of the metallic and ceramic constituent materials and the rule of mixtures are assumed, see Praveen and Reddy (1998) and Chakraborty *et al*. (2003). This results in a power law distribution over the cross-section of the Young modulus E and the Poisson ratio ν

$$f(y,z) = (f_1 - f_2)\left(\alpha_y y + \beta_y\right)^{n_y}\left(\alpha_z z + \beta_z\right)^{n_z} + f_2 \tag{12}$$

where f is the generic material property, α_y, α_z, β_y and β_z are defined according to the material reference system (this latter can differ from the global structural one) and n_y and n_z are the material gradation exponents. The divided differences $C_{ij}[\ldots;\ldots]$ in Eq. (9) are then computed from

$$\begin{aligned}
C_{11}(y,z) = C_{22}(y,z) = C_{33}(y,z) &= \frac{1-\nu(y,z)}{[1+\nu(y,z)][1-2\nu(y,z)]}E(y,z) \\
C_{12}(y,z) = C_{13}(y,z) = C_{23}(y,z) &= \frac{\nu(y,z)}{[1+\nu(y,z)][1-2\nu(y,z)]}E(y,z) \\
C_{44}(y,z) = C_{55}(y,z) = C_{66}(y,z) &= \frac{1}{2[1+\nu(y,z)]}E(y,z)
\end{aligned} \tag{13}$$

and Eq. (12). N_p equal to nine ensures the convergence of the results within the considered number of significant digits.

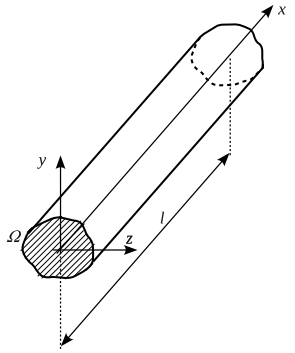

Fig. 1 Beam geometry and reference system

3. Hierarchical beam theories

The variation of the displacement field over the cross-section can be postulated a-priori. Several displacement-based theories can be formulated on the basis of the following generic kinematic field

$$\mathbf{u}(x,y,z) = F_\tau(y,z)\,\mathbf{u}_\tau(x) \quad \text{with} \quad \tau = 0,1,\ldots,N_u \tag{14}$$

N_u stands for the number of unknowns. It depends on the approximation order N. The compact expression is based on Einstein's notation: repeated indexes implicitly indicate summation. Thanks to this notation, problem's governing differential equations and boundary conditions can be derived in terms of a single 'fundamental nucleo'. The complexity related to higher than classical approximation terms is tackled and the theoretical formulation is valid for the generic approximation order and approximating functions $F_\tau(y,z)$. The approximating functions F_τ are Mac Laurin's polynomials. This choice is inspired by the classical beam models. N_u and F_τ as functions of N can be obtained through Pascal's triangle as shown in Table 1. The actual governing differential equations and boundary conditions due to a fixed approximation order are obtained straightforwardly via summation of the nucleo corresponding to each term of the expansion. According to the chosen polynomial functions, the generic N-order displacement field is:

$$\begin{aligned}
u_x &= u_{x1} + u_{x2}y + u_{x3}z + \ldots + u_{x\overline{N}}y^N + \ldots + u_{xN_{tot}}z^N \\
u_y &= u_{y1} + u_{y2}y + u_{y3}z + \ldots + u_{y\overline{N}}y^N + \ldots + u_{yN_{tot}}z^N \\
u_z &= u_{z1} + u_{z2}y + u_{z3}z + \ldots + u_{z\overline{N}}y^N + \ldots + u_{zN_{tot}}z^N \\
&\text{with } \overline{N} = \frac{N^2+N+2}{2} \text{ and } N_{tot} = \frac{(N+1)(N+2)}{2}
\end{aligned} \tag{15}$$

The kinematic field of a first-order theory is

$$\begin{aligned}
u_x &= u_{x1} + u_{x2}y + u_{x3}z \\
u_y &= u_{y1} + u_{y2}y + u_{y3}z \\
u_z &= u_{z1} + u_{z2}y + u_{z3}z
\end{aligned} \tag{16}$$

Classical Euler-Bernoulli's theory (EBT)

$$\begin{aligned}
u_x &= u_{x1} - u_{y1,x}y - u_{z1,x}z \\
u_y &= u_{y1} \\
u_z &= u_{z1}
\end{aligned} \tag{17}$$

and Timoshenko's theory (TBT)

$$\begin{aligned} u_x &= u_{x1} + u_{x2} y + u_{x3} z \\ u_y &= u_{y1} \\ u_z &= u_{z1} \end{aligned} \tag{18}$$

are straightforwardly derived from the first-order approximation model. It should be noted that the reduced Hooke law for the axial stress/strain relation

$$\sigma_{xx} = Q_{11} \varepsilon_{xx} \tag{19}$$

should be used for classical models. This is due to the fact that the kinematic fields in Eqs. (17) and (18) account for a rigid cross-section ($\varepsilon_{yy} = \varepsilon_{zz} = 0$) in clear violation of Poisson's effect

$$\varepsilon_{ii} = -\nu \varepsilon_{xx} \neq 0 \quad \text{with} \quad i = y, z \tag{20}$$

This incongruence in the theory, known as Poisson's locking, see Carrera and Brischetto (2008a, b), is avoided by assuming Eq. (19) instead of the full three dimensional Hooke equations. The reduced material stiffness coefficient Q_{11} is classically obtained imposing the equations in σ_{yy} and σ_{zz} in Hooke's law equal to zero. An algebraic linear system in ε_{yy} and ε_{zz} is, then, obtained. The reduced stiffness coefficients Q_{11} is derived by substituting its solution into Hooke's equations in σ_{xx}

$$Q_{11} = C_{11} + C_{12} \frac{C_{12} C_{33} - C_{13} C_{23}}{C_{23}^2 - C_{22} C_{33}} + C_{13} \frac{C_{22} C_{13} - C_{12} C_{23}}{C_{23}^2 - C_{22} C_{33}} \tag{21}$$

and, in the case of isotropic materials, Q_{11} is equal to the Young modulus E. In this last case, the reduced material stiffness law can be also obtained by replacing Eq. (20) within the Hooke equation in the normal stress components σ_{ii}. The equation in the axial stress yields Eq. (19) with $Q_{11} = E$ and the equations in the normal stresses σ_{yy} and σ_{zz} are equal to zero. It should be noted that the Hooke equations containing the shear stresses and strains are not reduced. No shear correction coefficient is considered for TBT, since it depends on several parameters, such as the geometry of the cross-section, see, for instance, Cowper (1966) and Murty (1970). Higher-order models yield a more detailed description of the shear mechanics (no shear correction coefficient is required), the in- and out-of-section deformations, the coupling of the spatial directions due to Poisson's effect and the torsional mechanics than classical models do. A more general description of the proposed model as well as a detailed investigation of the effectiveness of each expansion term in the a-priori kinematic field can be found in Carrera *et al*. (2011) and in Carrera and Petrolo (2011).

4. Governing equations

The governing differential equations and the boundary conditions are obtained via the Principle of Virtual Displacements, see Reddy (2002)

$$\delta L_i + \delta L_\rho = \delta L_e \tag{22}$$

δ stands for a variation, L_i represents the strain energy, L_e is the work done by the external loads and L_ρ is the inertial work.

4.1 Strain energy

Coherently with the stresses and strains grouping in Eqs. (2) and (3), the virtual strain energy results in a sum of two contributes

$$\delta L_i = \int_l \int_\Omega \left(\delta \boldsymbol{\varepsilon}_n^T \boldsymbol{\sigma}_n + \delta \boldsymbol{\varepsilon}_p^T \boldsymbol{\sigma}_p \right) d\Omega dx \tag{23}$$

By replacing the geometrical relations in Eq. (5), the material constitutive equations in Eq. (7) and the unified approximation of the displacement field in Eq. (14) and after integrating by parts, the previous equation reads

$$\begin{aligned} \delta L_i = & \int_l \delta \mathbf{u}_\tau^T \int_\Omega \left\{ \left(\mathbf{D}_{np} F_\tau \right)^T \left[\mathbf{C}_{np} \left(\mathbf{D}_p F_s \right) + \mathbf{C}_{nn} \left(\mathbf{D}_{np} F_s \right) + \mathbf{C}_{nn} F_s \mathbf{D}_{nx} \right] \right. \\ & \left(\mathbf{D}_p F_\tau \right)^T \left[\mathbf{C}_{pp} \left(\mathbf{D}_p F_s \right) + \mathbf{C}_{pn} \left(\mathbf{D}_{np} F_s \right) + \mathbf{C}_{pn} F_s \mathbf{D}_{nx} \right] \\ & \left. -\mathbf{D}_{nx}^T \left[\mathbf{C}_{np} F_\tau \left(\mathbf{D}_p F_s \right) + \mathbf{C}_{nn} F_\tau \left(\mathbf{D}_{np} F_s \right) + \mathbf{C}_{nn} F_\tau F_s \mathbf{D}_{nx} \right] \right\} d\Omega \mathbf{u}_s dx \\ & \delta \mathbf{u}_\tau^T \int_\Omega F_\tau \left[\mathbf{C}_{np} \left(\mathbf{D}_p F_s \right) + \mathbf{C}_{nn} \left(\mathbf{D}_{np} F_s \right) + \mathbf{C}_{nn} F_s \mathbf{D}_{nx} \right] d\Omega \mathbf{u}_s \Big|_{x=0}^{x=l} \end{aligned} \tag{24}$$

In a compact vectorial form

$$\delta L_i = \int_l \delta \mathbf{u}_\tau^T \tilde{\mathbf{K}}^{\tau s} \mathbf{u}_s dx + \delta \mathbf{u}_\tau^T \tilde{\Pi}^{\tau s} \mathbf{u}_s \Big|_{x=0}^{x=l} \tag{25}$$

The components of the differential stiffness matrix $\tilde{\mathbf{K}}^{\tau s}$ are

$$\begin{aligned} \tilde{K}_{xx}^{\tau s} &= J_{\tau_{,y} s_{,y}}^{66} + J_{\tau_{,z} s_{,z}}^{55} - J_{\tau s}^{11} \frac{\partial^2}{\partial x^2} & \tilde{K}_{xy}^{\tau s} &= \left(J_{\tau_{,y} s}^{66} - J_{\tau s_{,y}}^{12} \right) \frac{\partial}{\partial x} & \tilde{K}_{xz}^{\tau s} &= \left(J_{\tau_{,z} s}^{55} - J_{\tau s_{,z}}^{13} \right) \frac{\partial}{\partial x} \\ \tilde{K}_{yy}^{\tau s} &= J_{\tau_{,y} s_{,y}}^{22} + J_{\tau_{,z} s_{,z}}^{44} - J_{\tau s}^{66} \frac{\partial^2}{\partial x^2} & \tilde{K}_{yx}^{\tau s} &= \left(J_{\tau_{,y} s}^{12} - J_{\tau s_{,y}}^{66} \right) \frac{\partial}{\partial x} & \tilde{K}_{yz}^{\tau s} &= J_{\tau_{,y} s_{,z}}^{23} + J_{\tau_{,z} s_{,y}}^{44} \\ \tilde{K}_{zz}^{\tau s} &= J_{\tau_{,y} s_{,y}}^{44} + J_{\tau_{,z} s_{,z}}^{33} - J_{\tau s}^{55} \frac{\partial^2}{\partial x^2} & \tilde{K}_{zx}^{\tau s} &= \left(J_{\tau_{,z} s}^{13} - J_{\tau s_{,z}}^{55} \right) \frac{\partial}{\partial x} & \tilde{K}_{zy}^{\tau s} &= J_{\tau_{,z} s_{,y}}^{23} + J_{\tau_{,y} s_{,z}}^{44} \end{aligned} \tag{26}$$

The generic term $J_{\tau_{(,\phi)} s_{(,\xi)}}^{gh}$ is a cross-section moment

$$J_{\tau_{(,\phi)} s_{(,\xi)}}^{gh} = \int_\Omega C_{gh} F_{\tau_{(,\phi)}} F_{s_{(,\xi)}} d\Omega \tag{27}$$

As far as the boundary conditions are concerned, the components of $\tilde{\Pi}^{\tau s}$ are

$$\begin{aligned}
&\tilde{\Pi}_{xx}^{\tau s} = J_{\tau s}^{11}\frac{\partial}{\partial x} \quad \tilde{\Pi}_{xy}^{\tau s} = J_{\tau s,_y}^{12} \quad \tilde{\Pi}_{xz}^{\tau s}=J_{\tau s,_z}^{13} \\
&\tilde{\Pi}_{yy}^{\tau s}=J_{\tau s}^{66}\frac{\partial}{\partial x} \quad \tilde{\Pi}_{yx}^{\tau s} = J_{\tau s,_y}^{66} \quad \tilde{\Pi}_{yz}^{\tau s}=0 \\
&\tilde{\Pi}_{zz}^{\tau s} = J_{\tau s}^{55}\frac{\partial}{\partial x} \quad \tilde{\Pi}_{zx}^{\tau s} = J_{\tau s,_z}^{55} \quad \tilde{\Pi}_{zy}^{\tau s}=0
\end{aligned} \tag{28}$$

4.2 Virtual work of the external loads

The total external virtual work δL_e is considered as due to a generic surface load $p_{\phi\xi}$ and a generic line load $l_{\phi\xi}$ with $\phi = y$ and z and $\xi = x$, y and z

$$\delta L_e = \delta L_p + \delta L_l \tag{29}$$

The subscripts convention for a surface and line load component is the same as for the stresses: the first subscript stands for the normal to the plane of application, whereas the second one indicates the direction of the load itself. Surface loads act, therefore, over planes parallel to the plane xz or the xy one

$$\begin{aligned}
&p_{y\xi}(x):\xi = x,y,z \text{ at } y = \hat{y}_{p_{y\xi}}, \forall z \in \left[\hat{z}^-_{p_{y\xi}}, \hat{z}^+_{p_{y\xi}}\right] \\
&p_{z\xi}(x):\xi = x,y,z \text{ at } z = \hat{z}_{p_{z\xi}}, \forall y \in \left[\hat{y}^-_{p_{z\xi}}, \hat{y}^+_{p_{z\xi}}\right]
\end{aligned} \tag{30}$$

δL_p is

$$\delta L_p = \delta L_{p_{zz}} + \delta L_{p_{zx}} + \delta L_{p_{zy}} + \delta L_{p_{yy}} + \delta L_{p_{yx}} + \delta L_{p_{yz}} \tag{31}$$

The terms in Eq. (31) are

$$\begin{aligned}
&\left(\delta L_{p_{zx}}, \delta L_{p_{yx}}\right) = \int_l \delta u_{x\tau}\left(p_{zx}E_\tau^z, p_{yx}E_\tau^y\right)dx \\
&\left(\delta L_{p_{yy}}, \delta L_{p_{zy}}\right) = \int_l \delta u_{y\tau}\left(p_{yy}E_\tau^y, p_{zy}E_\tau^z\right)dx \\
&\left(\delta L_{p_{zz}}, \delta L_{p_{yz}}\right) = \int_l \delta u_{z\tau}\left(p_{zz}E_\tau^z, p_{yz}E_\tau^y\right)dx
\end{aligned} \tag{32}$$

with

$$E_\tau^y = \int_{\hat{z}^-_{p_{y\xi}}}^{\hat{z}^+_{p_{y\xi}}} F_\tau\left(\hat{y}_{p_{y\xi}}, z\right)dz \quad E_\tau^z = \int_{\hat{y}^-_{pz\xi}}^{\hat{y}^+_{pz\xi}} F_\tau\left(y, \hat{z}_{p_{z\xi}}\right)dy \tag{33}$$

The considered line loads are

$$l_{\phi\xi}(x):\phi = y,z,\xi = x,y,z \quad \text{at} \quad (y,z) = \left(\hat{y}_{l_{\phi\xi}}, \hat{z}_{l_{\phi\xi}}\right) \tag{34}$$

where $\left(\hat{y}_{l_{\phi\xi}}, \hat{z}_{l_{\phi\xi}}\right)$ are the cross-section coordinates of the application point. The external virtual

work is

$$\delta L_l = \delta L_{l_{zz}} + \delta L_{l_{zx}} + \delta L_{l_{zy}} + \delta L_{l_{yy}} + \delta L_{l_{yx}} + \delta L_{l_{yz}} \tag{35}$$

and in a explicit form

$$\begin{aligned}
\left(\delta L_{l_{zx}}, \delta L_{l_{yx}}\right) &= \int_l \delta u_{x\tau}\left[l_{zx}F_\tau\left(\hat{y}_{l_{zx}}, z_{l_{zx}}\right), l_{yx}F_\tau\left(\hat{y}_{l_{yx}}, z_{l_{yx}}\right)\right]dx \\
\left(\delta L_{l_{yy}}, \delta L_{l_{zy}}\right) &= \int_l \delta u_{x\tau}\left[l_{yy}F_\tau\left(\hat{y}_{l_{yy}}, z_{l_{zy}}\right), l_{zy}F_\tau\left(\hat{y}_{l_{zy}}, z_{l_{zy}}\right)\right]dx \\
\left(\delta L_{l_{zz}}, \delta L_{l_{yz}}\right) &= \int_l \delta u_{x\tau}\left[l_{zz}F_\tau\left(\hat{y}_{l_{zz}}, z_{l_{zz}}\right), l_{yz}F_\tau\left(\hat{y}_{l_{yz}}, z_{l_{yz}}\right)\right]dx
\end{aligned} \tag{36}$$

4.3 Inertial work

The virtual inertial work is

$$\delta L_\rho = \int_l \int_\Omega \rho \delta \mathbf{u}^T \ddot{\mathbf{u}} d\Omega dx \tag{37}$$

where ρ is the material density and double dots stand for the second time derivative (t stands for time). Replacing Eq. (14) within Eq. (37) yields

$$\delta L_\rho = \int_l \delta \mathbf{u}_\tau^T \int_\Omega \rho F_\tau F_s d\Omega \ddot{\mathbf{u}}_s dx = \int_l \delta \mathbf{u}_\tau^T \mathbf{M}^{\tau s} \ddot{\mathbf{u}}_s dx \tag{38}$$

The components of the inertial matrix $\mathbf{M}^{\tau s}$ are

$$M_{ij}^{\tau s} = \delta_{ij} \int_\Omega \rho F_\tau F_s d\Omega = \delta_{ij} J_{\tau s}^{\rho} \tag{39}$$

where δ_{ij} is Kronecker's delta and $J_{\tau s}^{\rho}$ is

$$J_{\tau s}^{\rho} = \int_\Omega \rho F_\tau F_s \, d\Omega \tag{40}$$

4.4 Governing equation fundamental nucleo

The explicit form of the fundamental nucleo of the governing equations is

$$\begin{aligned}
\delta u_{x\tau}: \quad & -J_{\tau s}^{11} u_{xs,xx} + \left(J_{\tau,z\,s,z}^{55} + J_{\tau,y\,s,y}^{66}\right) u_{xs} + \left(J_{\tau,y\,s}^{66} - J_{\tau s,y}^{12}\right) u_{ys,x} + \left(J_{\tau,z\,s}^{55} - J_{\tau s,z}^{13}\right) u_{zs,x} + J_{\tau s}^{\rho} \ddot{u}_{xs} = \\
& p_{zx}E_\tau^z + p_{yx}E_\tau^y + l_{zx}F_\tau\left(\hat{y}_{l_{zx}}, \hat{z}_{l_{zx}}\right) + l_{yx}F_\tau\left(\hat{y}_{l_{yx}}, \hat{z}_{l_{yx}}\right) \\
\delta u_{y\tau}: \quad & \left(J_{\tau,y\,s}^{12} - J_{\tau s,y}^{66}\right) u_{xs,x} - J_{\tau s}^{66} u_{ys,xx} + \left(J_{\tau,y\,s,y}^{22} + J_{\tau,z\,s,z}^{44}\right) u_{ys} + \left(J_{\tau,y\,s,z}^{23} + J_{\tau,z\,s,y}^{44}\right) u_{zs} + J_{\tau s}^{\rho} \ddot{u}_{ys} = \\
& p_{zy}E_\tau^z + p_{yy}E_\tau^y + l_{zy}F_\tau\left(\hat{y}_{l_{zy}}, \hat{z}_{l_{zy}}\right) + l_{yy}F_\tau\left(\hat{y}_{l_{yy}}, \hat{z}_{l_{yy}}\right) \\
\delta u_{z\tau}: \quad & \left(J_{\tau,z\,s}^{13} - J_{\tau s,z}^{55}\right) u_{xs,x} + \left(J_{\tau,z\,s,y}^{23} + J_{\tau,y\,s,z}^{44}\right) u_{ys} - J_{\tau s}^{55} u_{zs,xx} + \left(J_{\tau,z\,s,z}^{33} + J_{\tau,y\,s,y}^{44}\right) u_{zs} + J_{\tau s}^{\rho} \ddot{u}_{zs} = \\
& p_{zz}E_\tau^z + p_{yz}E_\tau^y + l_{zz}F_\tau\left(\hat{y}_{l_{zz}}, \hat{z}_{l_{zz}}\right) + l_{yz}F_\tau\left(\hat{y}_{l_{yz}}, \hat{z}_{l_{yz}}\right)
\end{aligned} \tag{41}$$

The essential and the natural boundary conditions are

$$\begin{gathered}\text{either } u_{x\tau} = \hat{u}_{x\tau} \text{ or } J_{\tau s}^{11} u_{xs,_x} + J_{\tau s,_y}^{12} u_{ys} + J_{\tau s,_z}^{13} u_{zs} = 0 \\ \text{either } u_{y\tau} = \hat{u}_{y\tau} \text{ or } J_{\tau s,_y}^{66} u_{xs} + J_{\tau s}^{66} u_{ys,_x} = 0 \\ \text{either } u_{z\tau} = \hat{u}_{z\tau} \text{ or } J_{\tau s,_z}^{55} u_{xs} + J_{\tau s}^{55} u_{zs,_x} = 0\end{gathered} \tag{42}$$

For a fixed approximation order, the nucleo has to be expanded over the indeces τ and s in order to obtain the governing equations and the boundary conditions of the desired model.

4.5 Strong form space domain solution

The differential equations are solved via a strong form, Navier-type solution. Within the approximation of the mechanical model, the solution is, therefore, exact. The following space-harmonic displacement field is adopted:

$$\begin{aligned}u_x(x,y,z;t) &= U_{x\tau}(t) F_\tau(y,z) \cos(\alpha x) \\ u_y(x,y,z;t) &= U_{y\tau}(t) F_\tau(y,z) \sin(\alpha x) \\ u_z(x,y,z;t) &= U_{z\tau}(t) F_\tau(y,z) \sin(\alpha x)\end{aligned} \tag{43}$$

By the nature of the solution, investigations are restrained to simply supported beams. Parameter α is

$$\alpha = \frac{m\pi}{l} \tag{44}$$

where $m \in N^*$ represents the half-wave number along the beam axis and $U_{i\tau}$ are the maximal amplitudes of the displacement components. It is assumed that the surface and line loads vary along *x* in the following manner

$$\begin{gathered}\left(p_{zz}, p_{yy}, p_{zy}, p_{yz}\right) = \left(P_{zz}, P_{yy}, P_{zy}, P_{yz}\right) \sin(\alpha x) \\ \left(p_{zx}, p_{yx}\right) = \left(P_{zx}, P_{yx}\right) \cos(\alpha x) \\ \left(l_{zz}, l_{yy}, l_{zy}, l_{yz}\right) = \left(L_{zz}, L_{yy}, L_{zy}, L_{yz}\right) \sin(\alpha x) \\ \left(l_{zx}, l_{yx}\right) = \left(L_{zx}, L_{yx}\right) \cos(\alpha x)\end{gathered} \tag{45}$$

where $P_{\phi\xi}$ and $L_{\phi\xi}$ are the maximal load amplitudes, which are function of time. The displacement field in Eq. (43) satisfies the Dirichlet boundary conditions for the displacement components u_y and u_z and a Robin type one along the axial direction since for $x = 0$ and l the following relations hold

$$u_{x,_x} = 0 \quad u_y = 0 \quad u_z = 0 \tag{46}$$

Upon substitution of Eq. (43) into Eq. (41), the fundamental algebraic nucleo for the forced

vibrations is obtained

$$\delta \mathbf{U}_\tau : \mathbf{M}^{\tau s} \ddot{\mathbf{U}}_s + \mathbf{K}^{\tau s} \mathbf{U}_s = \mathbf{P}_\tau \tag{47}$$

The components of the algebraic stiffness matrix $\mathbf{K}^{\tau s}$ are

$$\begin{aligned}
&K_{xx}^{\tau s} = \alpha^2 J_{\tau s}^{11} + J_{\tau_{,z} s_{,z}}^{55} + J_{\tau_{,y} s_{,y}}^{66} \qquad K_{xy}^{\tau s} = \alpha\left(J_{\tau_{,y} s}^{66} - J_{\tau s_{,y}}^{12} \right) \qquad K_{xz}^{\tau s} = \alpha\left(J_{\tau_{,z} s}^{55} - J_{\tau s_{,z}}^{13} \right) \\
&K_{yy}^{\tau s} = \alpha^2 J_{\tau s}^{66} + J_{\tau_{,y} s_{,y}}^{22} + J_{\tau_{,z} s_{,z}}^{44} \qquad K_{yx}^{\tau s} = \alpha\left(J_{\tau s_{,y}}^{66} - J_{\tau_{,y} s}^{12} \right) \qquad K_{yz}^{\tau s} = J_{\tau_{,y} s_{,z}}^{23} + J_{\tau_{,z} s_{,y}}^{44} \\
&K_{zz}^{\tau s} = \alpha^2 J_{\tau s}^{55} + J_{\tau_{,z} s_{,z}}^{33} + J_{\tau_{,y} s_{,y}}^{44} \qquad K_{zx}^{\tau s} = \alpha\left(J_{\tau s_{,z}}^{55} - J_{\tau_{,z} s}^{13} \right) \qquad K_{zy}^{\tau s} = J_{\tau_{,z} s_{,y}}^{23} + J_{\tau_{,y} s_{,z}}^{44}
\end{aligned} \tag{48}$$

4.6 Time domain solution

Upon expansion of the dynamic fundamental nucleo in Eq. (47) over the indeces τ and s, the final algebraic problem is obtained

$$\mathbf{M}\ddot{\mathbf{q}} + \mathbf{K}\mathbf{q} = \mathbf{P} \tag{49}$$

where $\mathbf{M}$, $\mathbf{K}$ and $\mathbf{P}$ are the global mass and stiffness matrix and the load vector and $\ddot{\mathbf{q}}$ and $\mathbf{q}$ are the unknown acceleration and displacement vectors. In the case of damping, Eq. (49) becomes

$$\mathbf{M}\ddot{\mathbf{q}} + \mathbf{C}\dot{\mathbf{q}} + \mathbf{K}\mathbf{q} = \mathbf{P} \tag{50}$$

being $\dot{\mathbf{q}}$ the velocity vector and $\mathbf{C}$ the damping matrix. The derivation of the damping matrix has not been presented in the previous subsections since the classical Rayleigh weighted formula is assumed

$$\mathbf{C} = \lambda \mathbf{M} + \kappa \mathbf{K} \tag{51}$$

where λ and κ are two real constants. A solution of the dynamic problem is obtained by means of the following time discretisation of displacements and velocities, see Newmark (1959)

$$\begin{aligned}
\mathbf{q}_{n+1} &= \mathbf{q}_n + \dot{\mathbf{q}}_n \Delta t + \frac{1}{2}\left[(1-2\beta)\ddot{\mathbf{q}}_n + 2\beta \ddot{\mathbf{q}}_{n+1} \right] \Delta t^2 \\
\dot{\mathbf{q}}_{n+1} &= \dot{\mathbf{q}}_n + \left[(1-\gamma)\ddot{\mathbf{q}}_n + \gamma \ddot{\mathbf{q}}_{n+1} \right] \Delta t
\end{aligned} \tag{52}$$

in which $(\ )_n$ and $(\ )_{n+1}$ stand for a quantity evaluated at time step t_n and t_{n+1}, with $\Delta t = t_{n+1} - t_n$. Parameters β and γ should be properly chosen in order to preserve accuracy and stability. The trapezoidal rule ($\beta = 1/4$ and $\gamma = 1/2$) is here used. It should be pointed out, as discussed in Newmark (1959), that a value of γ different than $1/2$ results in spurious damping. A linear algebraic system for time step t_{n+1} is obtained by replacing Eq. (10) within Eq. (8)

$$\left(\mathbf{M}+\gamma\mathbf{C}\Delta t+\beta\mathbf{K}\Delta t^2\right)\ddot{\mathbf{q}}_{n+1}=\mathbf{P}_n-\mathbf{C}\left[\dot{\mathbf{q}}_n+\left(1-\gamma\right)\ddot{\mathbf{q}}_n\Delta t\right]-\mathbf{K}\left[\mathbf{q}_n+\dot{\mathbf{q}}_n\Delta t+\left(1-2\beta\right)\ddot{\mathbf{q}}_n\frac{\Delta t^2}{2}\right] \quad (53)$$

As far as initial conditions are concerned, nil displacement and velocity vectors are assumed at initial time for the numerical investigations without loss of generality.

5. Numerical results and discussion

The beam support is $[0,l]\times[-a/2,a/2]\times[-b/2,b/2]$. Square cross-section with $a = b = 1$ m are considered. The length-to-side ratio l/a is equal to 100 and 10. Slender and deep beams are, therefore, investigated. FGMs beams are made of zirconia and aluminium. The mechanical properties of zirconia are: E_1 = 151 GPa, ν_1 = 0.28 and ρ_1 = 5700 kg/m^3. In the case of aluminium, the following mechanical properties are used: E_2 = 72 GPa, ν_2 = 0.33 and ρ_2 = 2800 kg/m^3. Young's modulus, Poisson's ratio and density vary along the cross-section axes according to the power gradation law in Eq. (12). Material reference system is coincident with the structural one. The coefficients in Eq. (12), therefore, are: $\alpha_y = a^{-1}$, $\alpha_z = b^{-1}$ and $\beta_y = \beta_z = 0.5$. Material exponents n_y and n_z are considered as analysis parameters. Without loss of generality, they are assumed to be as high as four and as low as 0.25. In such a manner, the cross-section corner $(+a/2,+b/2)$ is made of zirconia, whereas the material is fully aluminium at $(-a/2,-b/2)$, see Fig. 2. A surface and a line load are considered. They vary over time sinusoidally

$$\left(P_{yy},L_{yy}\right)=\left(\hat{P}_{yy},\hat{L}_{yy}\right)\sin\left(\omega_p t\right) \quad (54)$$

where $\hat{P}_{yy}$ and $\hat{L}_{yy}$ are the maximal amplitudes and ω_p is the load circular frequency (it is assumed to be equal to 8π rad/s). The time increment Δt is $5\cdot10^{-3}$ s, the final time (t_f) is 90 and two seconds for $l/a=100$ and ten, respectively. It should be noted that, since a Navier-type solution is used, the load varies sinusoidally along the beam axis with m in Eq. (44) equal to one. As far as validation is concerned, results are compared with three-dimensional FEM solutions obtained via the commercial code ANSYS. The three-dimensional quadratic element "Solid186" is used. Each element is considered as homogeneous by referring to the material properties at its centre point. Although the proposed closed form solution and the three-dimensional FEM one are different, some considerations about the computational cost can be done considering the degrees of freedom (DOFs) per cross-section. For the three-dimensional FEM solution (FEM-3D), the DOFs as function of the number of elements along z- or, equivalently, y-axis n are $3\left(3n+1\right)\left(n+1\right)$. For the considered solutions, n = 20 and the DOFs per cross-section are about 3850. For a fixed approximation order N, the DOFs of the proposed solutions are $3\left(N+1\right)\left(N+2\right)/2$. In the case of a fifth-order model, they are 63. This latter model ensures the convergence of the results for all the considered cases.

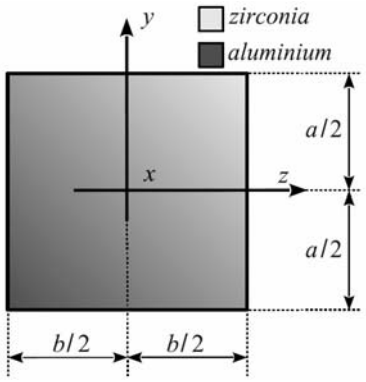

Fig. 2 Beam cross-section

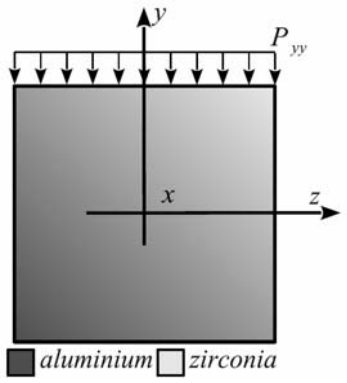

Fig. 3 Surface load P_{yy}

5.1 Surface load

The surface load is applied as shown in Fig. 3. Terms in Eqs. (30) are: $\hat{y}_{p_{yy}} = a/2$ and $\left(\hat{z}^{-}_{p_{yy}}, \hat{z}^{+}_{p_{yy}}\right) = \left(-b/2, +b/2\right)$. $\hat{P}_{yy} = -1$ Pa. The following displacements are considered

$$\tilde{u}_y = u_y\left(l/2, 0, 0\right) \quad \tilde{u}_x = u_x\left(0, a/2, 0\right) \quad \tilde{u}_z = u_z\left(l/2, a/2, b/2\right) \tag{55}$$

As a first case, damping is disregarded. Figs. 4 and 6 present the displacements time variation for both slender and deep beams. A linear material variation is considered along each cross-section direction ($n_y = n_z = 1$). In the case of a slender beam, results computed by EBT and fifth-order model are identical. For l / a =10, the two solutions diverge as time passes. This is clearly visible in Fig. 6(b). Some remarkable difference are also present at a time close to the initial one. For instance at $t = 0.130$ s, $\tilde{u}_y$ and $\tilde{u}_x$ computed via the two models differ by about 80% and 70%, respectively. A fifth-order model matches the reference FEM solution for all the considered cases, as shown by Figs. 4(b) and 5(b). For the sake of clarity, the three-dimensional FEM solution is presented only for $\tilde{u}_y$ and $\tilde{u}_x$ in the case of l / a =10. A mesh $20 \times 20 \times 20$ is considered. It

provides a good compromise between accuracy and computational costs. A convergence analysis is not here reported for the sake of brevity. Further details can be found in Giunta *et al*. (2010, 2011b). Fig. 7 shows the displacement components $\tilde{u}_y$ and $\tilde{u}_z$ for the material exponents as high as two and as low as 0.25. A perfect match between the fifth-order model and the reference FEM solution can be observed. The smaller the material exponent, the lower the amplitude of the oscillations. This is due to a higher presence of the stiffer ceramic phase. A second analysis is carried out accounting for damping. The damping coefficients are $\lambda = 2$ s^{-1} and $\kappa = 2 \cdot 10^{-4}$ s. Deep beams are investigated. The displacements components $\tilde{u}_y$ and $\tilde{u}_z$ are presented in Fig. 8. A bi-linear material gradation is considered. After a characteristic damping time, that is different for the two displacement components, the motion becomes similar to a sinusoidal. Fifth-order theory, TBT and FEM-3D yield coincident results for $\tilde{u}_y$. In the case of $\tilde{u}_z$, some differences between N = 5 and TBT can be observed. For this latter case, the solution FEM-3D (which is coincident with the fifth-order solution) is not presented for the sake of clearness of the figure. The absolute difference between TBT and N = 5 theory can be as high as about 10%. It is about 5% after stabilisation of the oscillations due to damping ($t > 1$ s).

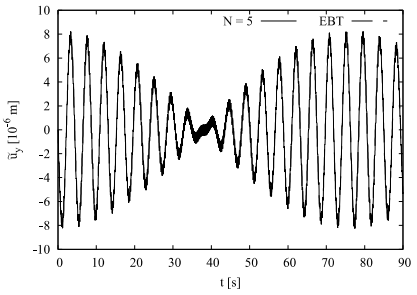

(a) $l/a = 100$

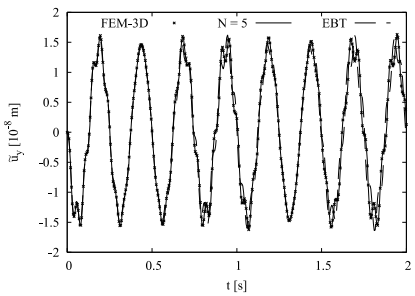

(b) $l/a = 10$

Fig. 4 Displacement component $\tilde{u}_y$ time variation, surface load P_{yy}, $n_y = n_z = 1$

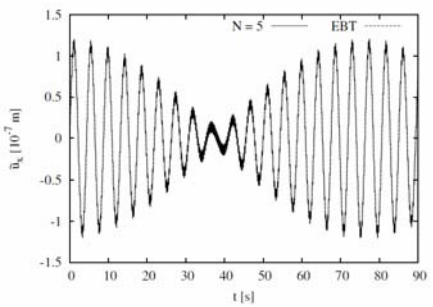

(a) $l/a = 100$

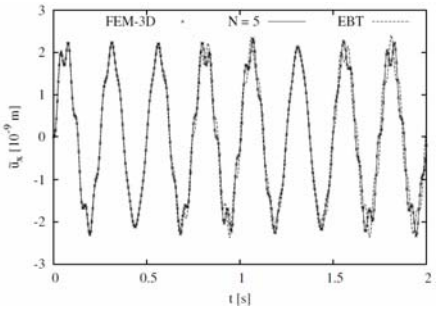

(b) $l/a = 10$

Fig. 5 Displacement component $\tilde{u}_x$ time variation, surface load P_{yy}, $n_y = n_z = 1$

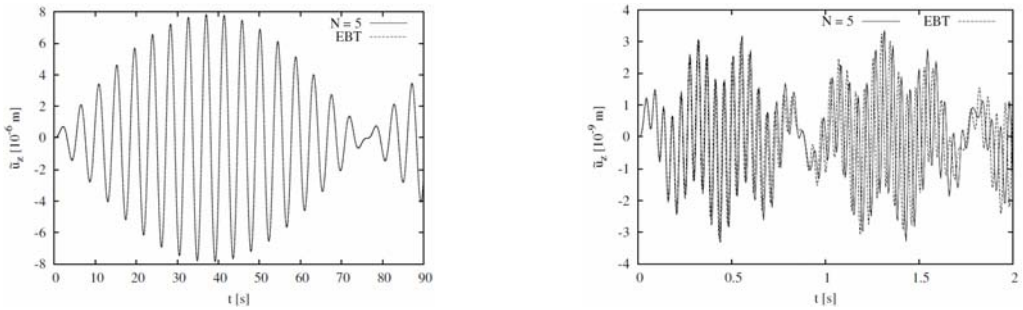

(a) $l/a = 100$ (b) $l/a = 10$

Fig. 6 Displacement component $\tilde{u}_z$ time variation, surface load P_{yy}, $n_y = n_z = 1$

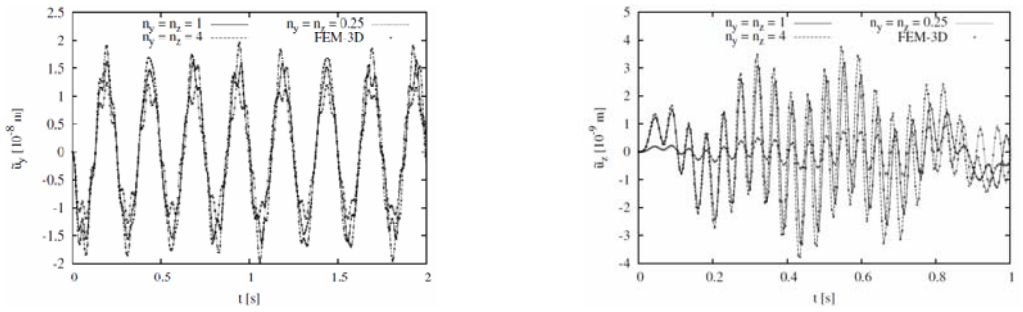

(a) $\tilde{u}_y$ (b) $\tilde{u}_z$

Fig. 7 Displacement components time variation for n_y = n_z = 4, 1 and 0.25 via fifth-order model and FEM-3D solution, surface load, l/a = 10

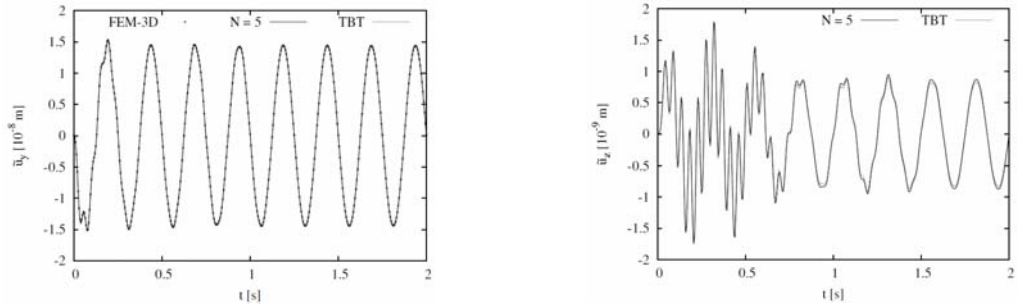

(a) $\tilde{u}_y$ (b) $\tilde{u}_z$

Fig. 8 Displacement components time variation, damping coefficients $\lambda = 2$ s^{-1} and $\kappa = 2 \cdot 10^{-4}$ s, surface load P_{yy}, $l/a = 10$

5.2 Line Load

The line load shown in Fig. 9 is considered. The load is applied at the cross-section corner $\left(\hat{y}_{l_{yy}}, \hat{z}_{l_{yy}}\right) = \left(-b/2, +b/2\right)$, and its amplitude is $\hat{L}_{yy} = +1$ Pa/m. This analysis aims at investigating the accuracy of the proposed models in the presence of localised loadings. A bi-linear material variation over the cross-section is considered and damping is disregarded. The cross-section displacement components $\tilde{u}_y$ and $\tilde{u}_z$ are evaluated at point $\left(l/2, -a/2, -b/2\right)$. The axial displacement is not presented for the sake of brevity. It is similar to $\tilde{u}_y$. A deep beam is considered since, as far as displacements are concerned, classical theories and higher-order models yield matching results for a slender beam. Results are presented in Figs. 10 and 11. FEM-3D solution has not been presented in the figures since it is coincident with the N = 5 model. A difference of about 10% is now present also in the case of $\tilde{u}_y$. This difference can be as high as 30% in the case of EBT. This is due to the fact that the deformation is not only governed by bending. Torsion is present and a localised deformation at the neighbourhood of the load application point, as shown in Giunta *et al*. (2010), is observable. These deformations cannot be accounted for by classical models since the cross-section is considered to be rigid on its-own plane.

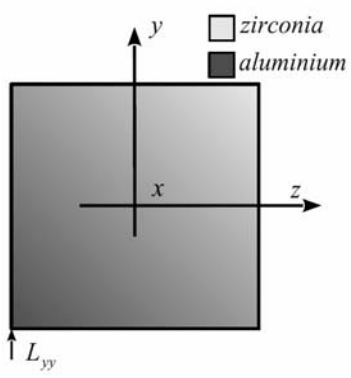

Fig. 9 Line load L_{yy}

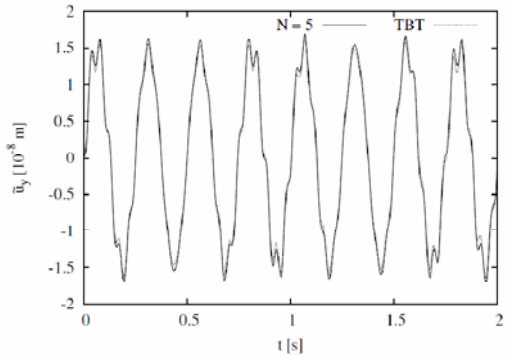

Fig. 10 Displacement component $\tilde{u}_y$ time variation for l/a = 10, line load L_{yy}, $n_y = n_z$ =1

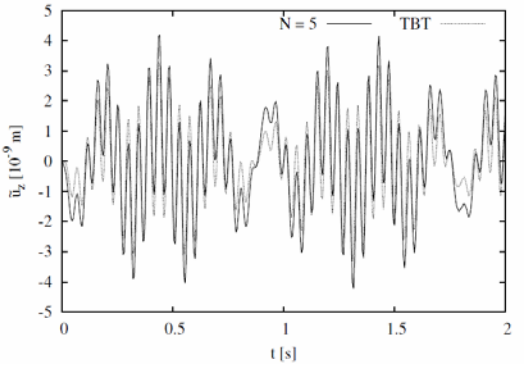

Fig. 11 Displacement component $\tilde{u}_z$ time variation for $l / a = 10$, line load L_{yy}, $n_y = n_z = 1$

Table 1 Mac Laurin's polynomials terms via Pascal's triangle

N	N_u	F_τ
0	1	$F_1 = 1$
1	3	$F_2 = y \;\; F_3 = z$
2	6	$F_4 = y^2 \;\; F_5 = yz \;\; F_6 = z^2$
3	10	$F_7 = y^3 \;\; F_8 = y^2 z \;\; F_9 = yz^2 \;\; F_{10} = z^3$
…	…	…
N	$\frac{(N+1)(N+2)}{2}$	$F^a_{\tilde{N}} = y^N \quad F_{\tilde{N}+1} = y^{N-1} z \quad \ldots \quad F^b_{N_{tot}-1} = yz^{N-1} \quad F_{N_{tot}} = z^N$

a: $\tilde{N} = \frac{1}{2}\left(N^2 + N + 2\right)$.

b: $N_{tot} = \frac{1}{2}(N+1)(N+2)$.

6. Conclusions

A dynamic analysis of functionally graded three-dimensional beams has been proposed. The beam models have been all derived via a unified formulation. Thanks to this formulation, higher-order models that account for non-classical effects such as shear deformations and in- and out-of-plane warping and localised deformations can be formulated straightforwardly. Euler-Bernoulli's and Timoshenko's classical models are obtained as particular cases. The governing differential equations have been solved exactly in space via a Navier-type solution, whereas Newmark's scheme has been used for the time domain solution. Simply supported beams subjected to surface and line loads have been investigated. Loads have been supposed to vary sinusoidally in time. The effect of several gradation exponents and of damping has been investigated. Results have been validated through comparison with three-dimensional FEM

solutions obtained via the commercial code ANSYS. Numerical investigation showed that, for the considered cases, the proposed formulation converges to the reference FEM solution. Very accurate results with a limited number of degrees of freedom have been obtained. It should be pointed out that a reduced numerical effort is particularly attractive in the cases where iterative solution schemes are required.

Acknowledgments

First and second authors are supported by the Fonds National de la Recherche Luxembourg via the CORE project C09/MS/05 FUNCTIONALLY and 787395/ASPIEZO, respectively.

References

Aboudi, J. (1991), *Mechanics of composite materials: a unified micromechanical approach*, Elsevier, The Netherlands.

Aboudi, J., Pindera, M.J. and Arnold, S.M. (1994), "Elastic response of metal matrix composites with tailored microstructures to thermal gradients", *Int. J. Solids Struct.*, **31**(10), 1393-1428.

Aboudi, J., Pindera, M.J. and Arnold, S.M. (1996), "Thermoelastic theory for the response of materials functionally graded in two directions", *Int. J. Solids Struct.*, **33**(7), 931-966.

Aboudi, J., Pindera, M.J. and Arnold, S.M. (1999), "Higher-order theory for functionally graded materials", *Compos. Part B Eng.*, **30**(8), 777-832.

Azadi, M. (2011), "Free and forced vibration analysis of FG beam considering temperature dependency of material properties", *J. Mech. Sci. Technol.*, **25**(1), 69-80.

Bathe, K.J. (2006), *Finite element procedures*, Prentice hall.

Birman, V. and Byrd, L.W. (2007), "Modeling and analysis of functionally graded materials and structures", *Appl. Mech. Rev.*, **60**(5), 195-216.

Bui, T. Q., Khosravifard, A., Zhang, Ch., Hematiyan, M.R. and Golub, M.V. (2013), "Dynamic analysis of sandwich beams with functionally graded core using a truly meshfree radial point interpolation method", *Eng. Struct.*, **47**, 90-104.

Carrera, E (2003), "Theories and finite elements for multilayered plates and shells: a unified compact formulation with numerical assessment and benchmarking", *Arch. Comput. Method. E.*, **10**(3), 215-296.

Carrera, E. and Brischetto, S. (2008a), "Analysis of thickness locking in classical, refined and mixed multilayered plate theories", *Compos. Struct.*, **82**(4), 549-562.

Carrera, E. and Brischetto, S. (2008b), "Analysis of thickness locking in classical, refined and mixed theories for layered shells", *Compos. Struct.*, **85**(1), 83-90.

Carrera, E. and Giunta, G. (2009a), "Hierarchical evaluation of failure parameters in composite plates", *AIAA J.*, **47**(3), 692-702.

Carrera, E. and Giunta, G. (2009b), "Exact, hierarchical solutions for localised loadings in isotropic, laminated and sandwich shells", *J. Pressure Vessel Technol.*, **131**(4), 041202.

Carrera, E. and Giunta, G. (2010), "Refined beam theories based on a unified formulation", *Int. J. Appl. Mech.*, **2**(1), 117-143.

Carrera, E., Giunta, G., Nali, P. and Petrolo, M. (2010), "Refined beam elements with arbitrary cross-section geometries", *Comput. Struct.*, **88**(5-6), 283-293.

Carrera, E., Giunta, G. and Petrolo, M. (2011), *Beam structures: classical and advanced theories*, Wiley-Blackwell.

Carrera, E. and Petrolo, M. (2011), "On the effectiveness of higher-order terms in refined beam theories", *J.*

Appl. Mech. - T ASME, **78**(2), 021013-1-021013-17.
Carrera, E. and Varello, A. (2013), "Dynamic response of thin-walled structures by variable kinematic one-dimensional models", *J. Sound Vib.*, **331**(24), 5268-5282.
Chakraborty, A., Gopalakrishnan, S. and Reddy, J.N. (2003), "A new beam finite element for the analysis of functionally graded materials", *Int. J. Mech. Sci.*, **45**(3), 519-539.
Cowper, G.R. (1966), "The shear co-efficient in Timoshenko beam theory", *Int. J. Appl. Mech.*, **33**(10), 335-340.
Giunta, G., Belouettar, S. and Carrera, E. (2010), "Analysis of FGM beams by means of classical and advanced theories", *Mech. Adv. Mater. Struct.*, **17**(8), 622-635.
Giunta, G., Biscani, F., Belouettar, S. and Carrera, E. (2011a), "Analysis of thin-walled beams via a one-dimensional unified formulation", *Int. J. Appl. Mech.*, **3**(3), 407-434.
Giunta, G., Biscani, F., Belouettar, S. and Carrera, E. (2011b), "Hierarchical modelling of doubly curved laminated composite shells under distributed and localised loadings", *Compos. Part B: Eng.*, **42**(4), 682-691.
Giunta, G., Crisafulli, D., Belouettar, S. and Carrera, E. (2011), "Hierarchical theories for the free vibration analysis of functionally graded beams", *Compos. Struct.*, **94**(1), 68-74.
Giunta, G., Biscani, F., Belouettar, S., Ferreira, A.J.M. and Carrera, E. (2013a), "Free vibration analysis of composite beams via refined theories", *Compos. Part B: Eng.*, **44**(1), 540-552.
Giunta, G., Crisafulli, D., Belouettar, S. and Carrera, E. (2013b), "A thermo-mechanical analysis of functionally graded beams via hierarchical modelling", *Compos. Struct.*, **95**, 676-690.
Hill, R. (1965), "A self-consistent mechanics of composite materials", *J. Mech. Phys. Solids*, **13**(4), 213-222.
Hughes, T.J.R. (2000), *The finite element method*, Dover.
Khalili, S.M.R., Jafari, A.A. and Eftekhari, S.A. (2010), "A mixed Ritz-DQ method for forced vibration of functionally graded beams carrying moving loads", *Compos. Struct.*, **92**(10), 2497-2511.
Koizumi, M. (1997), "FGN activities in Japan", *Compos. Part B – Eng.*, **28**(1-2), 1-4.
Miyamoto, Y., Kaysser, W. A., Rabin, B.H., Kawasaki, A. and Ford R.G. (1999), *Functionally graded materials: design*, *Processing and Applications*, Kluwer Academic, Boston, USA.
Mori, T. and Tanaka, K. (1973), "Average stress in matrix and average elastic energy of materials with misfitting inclusions", *Acta Metallurgica*, **21**(5), 571-574.
Murty, A.V. K. (1970), "Analysis of short beams", *AIAA J.*, **8**, 2098-2100.
Na, S., Kim, K.W. Lee, B.H. and Marzocca, P. (2009), "Dynamic response analysis of rotating functionally graded thin-walled blades exposed to steady temperature and external excitation", *J. Therm. Stresses*, **32**(3), 209-225.
Nemat-Nasser, S. and Hori, M. (1993), *Micromechanics: overall properties of heterogeneous materials*. North-Holland, New York.
Newmark, N.M. (1959), "A method of computation for structural dynamics", *J. Eng. Mech. - ASCE*, **85**(7), 67-94.
Philips, G.M. (2003), *Interpolation and approximation by polynomials*, Springer-Verlag.
Pindera, M. J., Aboudi, J. and Arnold, S.M. (1995), "Limitations of the uncoupled RVE-based micromechanical approach in the analysis of functional graded composites", *Mech. Mater.*, **20**(1), 77-94.
Praveen, G.N. and Reddy, J.N. (1998), "Nonlinear transient thermoelastic analysis of functionally graded ceramic-metal plates", *Int. J. Solids Struct.*, **35**(33), 4457-4476.
Reddy, J. N. (2002), *Energy principles and variational methods in applied mechanics*, John Wiley and Sons.
Shooshtari, A. and Rafiee, M. (2011), "Nonlinear forced vibration analysis of clamped functionally graded beams", *Acta Mech.*, **221**(1-2), 23-38.
Şimşek, M., and Kocatürk, T. (2009), "Free and forced vibration of a functionally graded beam subjected to a concentrated moving harmonic load", *Compos. Struct.*, **90**(4), 465-473.
Şimşek, M. (2010), "Vibration analysis of a functionally graded beam under a moving mass by using different beam theories", *Compos. Struct.*, **92**(4), 904-917.
Şimşek, M. and Cansiz, S. (2012), "Dynamics of elastically connected double-functionally graded beam systems with different boundary conditions under action of a moving harmonic load", *Compos. Struct.*,

94(9), 2861-2878.
Şimşek, M., Kocatürk, T. and Akbaş, Ş.D. (2012), "Dynamic behavior of an axially functionally graded beam under action of a moving harmonic load", *Compos. Struct.*, **94**(8), 2358-2364.
Suresh, S. and Mortensen, A. (1998), *Fundamentals of functional graded materials*, IOM Communications Limited, London, UK.
Wakashima, H. T. and Tsukamoto, H. (1990), "Micromechanical approach to the thermomechanics of ceramic-metal gradient materials", *Proceedings of the 1st Symposium on Functionally Gradient Materials, The Functionally Gradient Materials Forum,* Sendai, Japan.
Watanabe, R., Nishida, T. and Hirai, T. (2003), "Present status of research on design and processing of functionally graded materials", *Metal. Mater. Int.*, **9**(6), 513-519.
Yang, J., Chen, Y., Xiang, Y. and Jia. X.L. (2008), "Free and forced vibration of cracked inhomogeneous beams under an axial force and a moving load", *J. Sound Vib.*, **312**(1-2), 166-181.
Zienkiewicz, O.C., Taylor, R.L. and Zhu, J.Z. (2005), *The finite element method: its basis and fundamentals*, Elsevier.
Zuiker, J.R. and Dvorak, G.J. (1994), "The effective properties of functionally graded composites - i extension of the Mori-Tanaka method to linearly varying fields", *Compos. Eng.*, **4**(1), 19-35.

FC